Applied Surface Science 612 (2023) 155799

Contents lists available at ScienceDirect

Applied Surface Science

journal homepage: www.elsevier.com/locate/apsusc

Full Length Article

Biocompatible and antimicrobial multilayer fibrous polymeric wound dressing with optimally embedded silver nanoparticles

Nandini Sarviya [a,b,1], Urbashi Mahanta [a,c,1], Alexander Dart [a], Jyotsnendu Giri [b], Atul Suresh Deshpande [c], Mudrika Khandelwal [c], Mrinal Bhave [a], Peter Kingshott [a,d,*]

[a] Department of Chemistry and Biotechnology, Swinburne University of Technology, Hawthorn, Victoria, 3122, Australia
[b] Department of Biomedical Engineering, Indian Institute of Technology Hyderabad, India
[c] Department of Materials Science and Metallurgic Engineering, Indian Institute of Technology Hyderabad, India
[d] ARC Training Centre Training Centre in Surface Engineering for Advanced Materials (SEAM), Swinburne University of Technology, Hawthorn, Victoria 3122, Australia

ARTICLE INFO

Keywords:
Electrospinning
Ultrafine fiber
Silver nanoparticle
Antibacterial
Cell attachment and wound healing

ABSTRACT

The demand for advanced, biocompatible wound dressings with antibacterial properties is increasing in order to treat people with severe skin wounds, such as burn victims or those suffering from ulcers. We have developed an ultrafine three-layer polymer nanofiber mesh using electrospinning that is able to kill bacteria (*Escherichia coli; E. coli and Staphylococcus aureus; S. aureus*) but also has cytocompatibility properties. The first layer was generated with polystyrene (PS) for strength and functions as a carrier layer. The second layer consisted of polycaprolactone (PCL) with silver nanoparticles (Ag NPs) that were added to the spinning solution, which had antibacterial properties. Finally, the third layer comprised of polyethylene oxide (PEO) acting as a hydrophilic, barrier layer that was also non-adhesive, with the potential to further assist in wound healing. Systematic physicochemical and biological characterization was performed including dynamic light scattering (DLS), UV spectroscopy, X-ray photoelectron spectroscopy (XPS), X-ray diffraction (XRD), inductively coupled plasma optical emission spectroscopy (ICP-OES), scanning electron microscopy (SEM), water contact angles, evaluation of antibacterial properties, and cell attachment and proliferation assays. The cumulative Ag ion release was optimized for a period up to 84 days in physiologically similar media at physiological temperature. Chemical, mechanical, and biological analysis demonstrated that incorporation of Ag NPs at higher quantities into the PCL fibers layer providing excellent antimicrobial activity with minimal toxicity at low concentration. The findings highlight the importance of optimizing the properties of Ag based antibacterial meshes to find the balance between high antibacterial activity and low toxicity.

1. Introduction

Skin wounds can be divided into two categories: (i) acute wounds, which occur from surgical procedures, traumas, radiation exposure, and superficial burns, and (ii) chronic wounds which are formed because of specific diseases and include diabetic pressure ulcers, and venous leg ulcers [1]. According to a US retrospective analysis in 2019 concerning Medicare beneficiaries, ~8.2 million people were identified as suffering from wounds with or without infections. Additionally, a review published in 2009 outlined the state of human skin wounds and the threat to both public health and the health care economy, and provided an overview of the future impact of acute and chronic wounds [2]. Furthermore, a 2018 market report predicted the annual global wound care product market will exceed 15 billion USD by 2022, increasing to 22 billion USD by 2024 [2]. The standard practice in wound care consists of removal of non-viable tissue to promote cell proliferation, in addition to swabbing and cleaning the wound area to treat infection. Finally, a dressing to both protect the wound from infection and to enhance the healing process is the target of current technology developments [3]. Over the past decade, electrospinning has become a popular method for the preparation of biomimicking scaffolds containing antimicrobial and anti-inflammatory agents, growth factors, and anesthetics to promote wound healing [1,3,4].

Electrospinning techniques have been used to fabricate fibrous

* Corresponding author at: Department of Chemistry and Biotechnology, Swinburne University of Technology, Hawthorn, VIC 3122, Australia.
E-mail address: pkingshott@swin.edu.au (P. Kingshott).
[1] Equal first authors.

https://doi.org/10.1016/j.apsusc.2022.155799
Received 13 September 2022; Received in revised form 17 November 2022; Accepted 18 November 2022
Available online 24 November 2022

scaffolds made from various polymers [5,6]. The fibrous wound healing scaffolds have been shown to promote wound care more effectively compared to traditional bandages because they closely resemble the native structure of the extra-cellular matrix (ECM), they have large surface area to volume ratios for efficient drug delivery, are highly porous, and can be highly multi-functional [6–8]. Additionally, their biomimicking properties can enhance fibroblast attachment, growth, and migration, simultaneously stimulating skin tissue regeneration at the wound site [5,9,10].

Synthetic polymers such as polystyrene (PS) [11], polycaprolactone (PCL) [7,8,12], and polyethylene oxide (PEO) [12] have been used to make fibrous scaffolds and are approved for many biomedical applications including topical wound healing and deep cut wound fillers. PS is used as a hydrophobic elastomeric flexible support, and pressure sensitive adhesive for wound dressings or mats, and is used as a preliminary filter for partial protection from the invasion of microorganisms [11,13]. PCL is a semi-crystalline biodegradable, hydrophobic, and biocompatible polymer [12,14]. PCL is elastic and has robust mechanical and physical properties, which creates a protective barrier against the external environment preventing displacement from the site of application by any kind of body movement [14]. Another advantage of PCL is its versatility in electropinning that also allows the loading of various drugs or other active agents into the fiber system [15]. Also, the nanoporous structure of PCL electrospun mats helps absorb moisture from wound surfaces, and allows strong adherence to the wound surroundings [16]. Void pores facilitate the infiltration and migration of cells into the fibrous mat, and removing the fibrous mat can tear the newly formed tissue, which leads to delays in the healing process [16]. To prevent dressing removal-based damage, coating of electrospun fiber mats using other non-adhesive biomaterials has been explored, since they do not compromise the mechanical and elastic properties of the fibrous dressing [16]. A variety of polymers are used as coating layers, applied using various techniques, and include gelatin, collagen, polyvinyl alcohol (PVA), or polyethylene oxide (PEO) [17–21]. PEO has been of great interest due to its biocompatibility and fiber forming properties [20]. It is well established for use in various biomedical applications such cartilage tissue regeneration and also wound dressings [20,22,23]. Moreover, PEO, by itself or combined with other polymers, has good fiber forming properties when made by electrospinning [23–25].

Recent advances in nanotechnology and tissue engineering have generated new possibilities in wound healing and tissue regeneration applications. Over the last two decades incorporation of antimicrobial agents and therapeutics into fibers, to improve wound healing outcomes, has been intensely studied, and new research is exploring innovative techniques to deliver the bioactive molecules [21,26,27]. Ag NPs are known for their intrinsic antimicrobial properties, with and without any other biomaterials [27–29]. The nanoparticles release the positively charged silver ion, that targets bacteria in several ways including binding to the membranes of bacteria leading to the disruption of respiratory processes, and interacting with DNA in inhibit cell division and cause bacterial death [29–31]. Thus, Ag NPs possess antibacterial properties against a wide range of pathogens [30–32].

In this work, systematic characterization and evaluation of a multilayered polymeric fibrous wound dressing with embedded Ag NPs made by electrospinning was performed. The Ag NPs and each layer of the electrospun fibrous dressing was characterized in detail using a range of analytical techniques including dynamic light scattering (DLS). for Ag particle size determination, fiber morphological determination using scanning electron microscope (SEM), presence of Ag in the fibrous dressing using ultraviolet (UV) spectroscopy, Ag ion release using Inductively coupled plasma optical emission spectroscopy (ICP-OES), crystallinity using X-ray diffraction (XRD), and surface chemistry using Fourier transform infrared (FTIR) and X-ray photoelectron spectroscopy (XPS). The effects of Ag NP concentration on fiber diameter was determined using SEM. Antibacterial properties of the fabricated fibrous dressings were systematically studied using the disc diffusion method in addition to zone of inhibition experiments with *E. coli* and *S. aureus*. *In vitro* cell experiments were performed with L-929 mouse fibroblasts to determine the toxicity and cell compatibility on the fibrous dressings.

2. Materials and methods

2.1. Materials

Polystyrene (PS, 110,000 g/mol, Sigma Aldrich), polycaprolactone (PCL, 80,000 g/mol), polyethylene oxide (PEO, 90,000 g/mol), silver nitrate ($AgNO_3$), chloroform, dimethylformamide (DMF), nutrient agar medium were all purchased from Sigma Aldrich, USA. Silver standard substrate, L-929 cell line, DMEM, fetal bovine serum (FBS), Trypsin solution (0.25%), Penicillin-streptomycin solution, Fungizone antimycotic solution, Phosphate Buffer Saline (1X PBS, 7.4 pH), live/dead assay kit, T75 flask, treated and non-treated 24 well plates were purchased from ThermoFisher Scientific, India. [3-(4,5-dimethylthiazol-2-yl)-5-(3-carboxymethoxyphenyl)-2-(4-sulfophenyl)–2H-tetrazolium] (MTS) assay kit (ab197010) was procured from Abcam. Deionised (DI) water obtained by Evaqua, MilliQ system, was used throughout the experiments.

2.2. Synthesis of silver nanoparticles (Ag NPs)

For the synthesis of Ag NPs, $AgNO_3$ was used as a precursor material and DMF was used as a reducing agent. In the process, 4 mg of $AgNO_3$ was added to 8 mL DMF solvent under constant stirring at 550 rpm overnight at room temperature. The solution was stirred until a colour change was observed in the mixture. The solvent reduces $AgNO_3$ to Ag^+ ion which is evident from the formation of dark brown to the black colour solution. Stored the solution in an airtight glass vial at 4 °C for further characterization.

2.3. Preparation of solution for electrospinning

Polymeric solutions were prepared using polystyrene (PS), PCL (with 0, 1, 2 and 5% Ag NPs) and polyethylene oxide (PEO) in chloroform: DMF (7:3). Briefly, 3 gm of PS (for 30%), 1.2 gm of PCL (for 12% w/v), with and without different concentration of Ag NPs (0, 1, 2 and 5% with respect to PCL), and 0.5 gm of PEO (for 5%) with and without 5% sugar (placebo drug), were prepared separately in 7:3 v/v chloroform and DMF (99%+ purity). After adding polymer, solutions were stirred for 6–8 h at room temperature to obtain homogeneous solutions. Determination of the electrical conductivity and viscosity was made using the four point probe method and a viscometer, respectively. The homogeneous polymeric solutions were then transferred into separate 10 mL syringes and loaded into a syringe pump.

2.4. Fabrication of multilayer fibrous bandages

Obtained homogeneous solutions of 30% PS, 12% PCL, with and without Ag NP, and 5% PEO were used to fabricate multilayer fibrous bandages using the electrospinning technique [33]. Briefly, prepared homogenous solutions were transferred into separate 10 mL syringes and loaded on separate syringe pumps with blunt end needles (needle diameter of 20G) and a flow rate of 1 mL/hour. The electrospinning instrument was prepared to collect each polymer layer and the voltage was set at 15 kV with a distance between the needle tip and aluminium foil-coated collector of 15 cm. PEO fibers were collected first on the ground piece of aluminium foil, which was placed on collector, allowing the PCL fibers (with and without 0, 1, 2 and 5% Ag NP) to deposit on the PEO fibers, followed by PS fiber deposition. The collected multilayer fibrous bandages were dried in a vacuum oven overnight at room temperature and stored at 4 ℃ for further characterization.

2.5. Characterization

All the experiments and analysis were performed in triplicate. Samples size of 1x1 cm (10 mg) for each and every experiment and analysis was used.

2.5.1. Morphology and size distribution of fibers

The morphology of the electrospun fibers were studied using a JEOL, JSM-7800F scanning electron microscope (SEM). The operating voltage of 5 kV was used. For size distribution of fibers, Image J software was used and an average of 50 fibers was used for statistical significance.

2.5.2. Particle size distribution

Particle size distribution of Ag NPs was measured dynamic light scattering (DLS). The average hydrodynamic diameter and polydispersity index were determined using the number average.

2.5.3. UV spectroscopy

UV absorbance of PCL solution with and without Ag NPs of different concentration was measured using PerkinElmer LAMBDA 365 spectrophotometer. In cooperation, absorbance and reflectance approaches were used in the wavelength range of 200 nm to 700 nm.

2.5.4. X-ray diffraction pattern (XRD)

XRD was performed on the electrospun fibers with and without Ag NPs to determine the crystal structure. XRD patterns of different electrospun fiber samples were recorded using a Bruker D8 Advance diffractometer using Cu Kα radiation ($\lambda = 1.54$ Å). Diffraction intensities were measured from 20° to 80° of 2θ angles at a scan speed of 1.2° per min with an increment of 0.02°.

2.5.5. Fourier transform infrared (FTIR) analysis

To determine the presence and interference of Ag NPs with PCL in different electrospun fibers, FTIR spectra was recorded using a Bruker FTIR, TENSOR 37. The different samples were mixed with dry KBr powder and pressed into a thin pallet under pressure (5000–10000 psi). The pellet was used to record FTIR spectra in the range of 400 to 4000 cm^{-1} with a 2 cm^{-1} resolution.

2.5.6. Inductively coupled plasma optical emission spectroscopy (ICP-OES)

The release of Ag ions from the fibrous mats were measured using ICP-OES (Bruker Aurora M90). To determine the release of Ag ions, 50 mg of fibrous mats with different concentrations of Ag NPs were incubated in simulated body fluid (SBF) at 37 °C and 7.4 pH for 84 days. Samples at different time points were collected and the released concentration was recorded using ICP-OES. For all measurements, the ICP-OES instrument was initialized, optimized, and calibrated as per manufacturer's instruction.

2.5.7. Degradation study

Degradation study of different fibrous bandages was performed in phosphate-buffered saline (PBS) solution containing gentamycin as reported previously [34]. Briefly, 100 mg of different fibrous samples with and without Ag NPs were placed in 5 mL PBS containing 50 μg mL^{-1} of gentamycin and then incubated at 37 °C with 70 rpm for 84 days. Buffer medium was renewed on every 3rd day. After every-two weeks interval, the lyophilized sample was analysed by weight variation and differences in the initial weight of sample (W_a) used for the degradation study and weight of degraded lyophilized sample (W_b) were calculated. The rate of degradation of fibrous bandages was calculated in % by the equation given below.

$$\textit{Degradation of fibrous bandages}\ (\%) = [(\boldsymbol{Wa} - \boldsymbol{Wb})/\boldsymbol{Wa}]*100$$

2.5.8. Water contact angles

Water contact angles was measured using a FTA1000 Drop Shape Analysis System, UK. A water volume of 5 μL was used in each measurement.

2.5.9. X-ray photoelectron spectroscopy (XPS)

XPS was used to determine the chemical composition of the electrospun fibers. It was measured using a Kratos Analytical Axis Nova spectrometer (Kratos Analytical, UK). For analysing the samples, a monochromated aluminium X-ray source ($Al_{k\alpha}$, $h\nu = 1486.6$ eV), operating at 15 mA current and 15 kV voltage (225 W), was used to determine the elemental composition from survey spectra (0 – 1200 eV) with a detector pass energy of 160 eV. High-resolution C1s and Ag 3d spectra (pass energy 20 eV) were used to determine the individual chemical components. Fiber samples (pieces of size 10*10 mm) were analysed in triplicate with 3 scans per sample and the atomic concentrations of elements were determined using the integral peak intensities and sensitivity factors as per instrument manufacturer. Standard operating conditions for the filament current were 1.8 Å, charge balance 3.3 V and 1.3 V bias voltage. Resultant spectra were analysed using CasaXPS analysis software (Version 2.3.18PR1.0) (Casa Software ltd. Teignmouth, UK).

2.5.10. Surface area and pore size analysis

Brunauer-Emmett-Teller (BET) and Barrett-Joyner-Halenda (BJH) techniques were used to find the specific surface area, pore characteristics, such as pore volume, and pore radius of the fiber materials based on N_2 adsorption–desorption measurements. The BET isotherm forms as a result of the amount of gas adsorbed relative to gas pressure. Nitrogen adsorption and desorption isotherms for all the samples were carried out using a Quantachrome ASiQwin instrument. The degassing temperature of 50 °C for 12 h was used for all the samples.

2.6. Antibacterial activity

The antibacterial activity of the fibers with and without Ag NPs was tested against clinical *Escherichia coli (E. coli) and Staphylococcus aureus (S. aureus)* isolates. One colony from a fresh culture of *E. coli* was taken and inoculated in 10 mL of nutrient broth followed by incubation at 37 °C for 18 h. The bacterial suspension was washed with sterile phosphate buffer solution (PBS) and resuspended again in a sterile nutrient broth. This solution was serially diluted to achieve a stock solution of 10^6 CFU/mL by matching the absorbance value with 0.5 McFarland standard solution. This bacterial solution was used to determine the minimum inhibitory concentration (MIC), zone of inhibition (ZOI) and time dependent inhibition activity of different fibers with and without Ag NPs.

2.6.1. Minimum inhibitory concentration

To determine the minimum inhibitory concentration of Ag NPs, bacterial cells were incubated with Ag NPs in Mueller-Hinton broth. Briefly, 100 μL of different concentrations of Ag NP solution (0 to 100 μg/mL) was transferred into 96 well plates, and 100 μL of bacterial cells with 10^6 CFU/mL concentration was added into each well containing the samples. Samples containing bacterial cells were incubated in a shaking incubator at 37 °C for 24 h. Post-incubation, the absorbance of bacterial cell cultures with samples was measured using a plate reader (Molecular Devices, SpectraMax iD5, USA) at 600 nm.

2.6.2. Zone of inhibition

Zone of inhibition of different fibrous samples was determined according to a reported method [35]. Briefly, 100 μL of *E. coli* and *S. aureus* stock suspension (10^6 CFU/mL) was spread on agar plates and samples with and without different Ag NP concentrations were placed on top. A control sample without Ag NPs was used as the negative control. The agar plates containing samples were incubated at 37 °C for 24 h. The antibacterial activity was measured by determining the zone of inhibition.

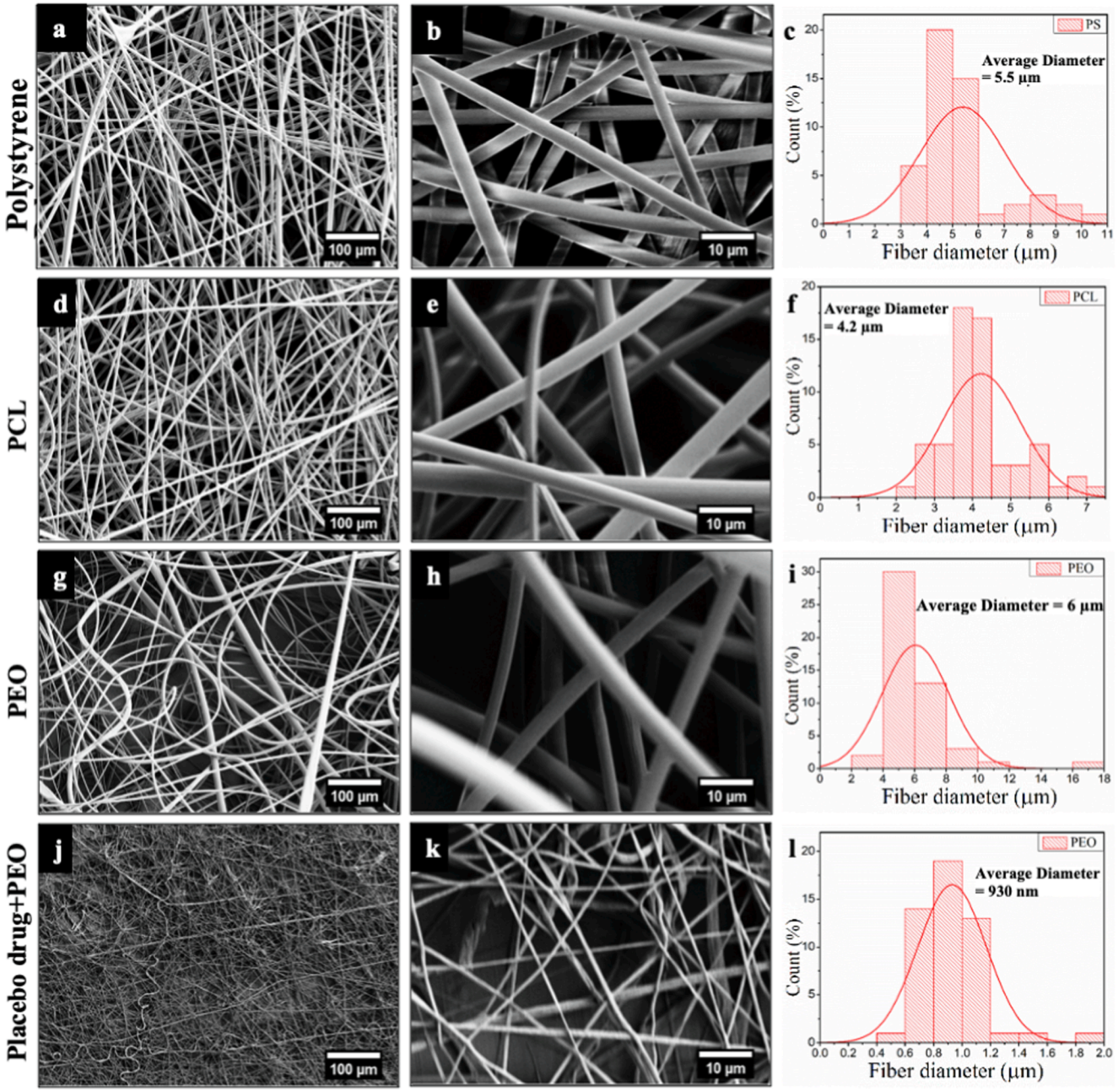

Fig. 1. SEM images of different layers of bandage fabricated using electrospinning. **(a-c)** outer layer fabricated using polystyrene, **(d-e)** middle layer was fabricated of PCL and **(g-l)** inner layer contained PEO without **(g-i)** and with **(j-l)** placebo drug. The fiber size distribution was calculated for each electrospun layer (c, f, i & l). Scale bars are 100 µm (a, d, g and k) and 10 µm (b, e, h and k).

2.6.3. *Time dependent inhibition activity*

Time dependent microorganism inhibition capabilities of the different fibers with and without Ag NPs was determined for different time points. Briefly, all samples were cut into 1x1 cm pieces and transferred to 24 well plates. Samples were washed twice with sterile PBS followed by washing with nutrient broth. 1 mL of *E. coli* and *S. aureus* stock suspension (10^6 CFU/mL) was added into each sample well and incubated for different time points (0, 2, 4, 8, 12 and 24 h). After every time point the optical density for each sample was measured using a plate reader at 600 nm.

2.7. *Cell culture, cell attachment, viability, and metabolic activity*

L-929 mouse fibroblasts was procured from ThermoFisher Scientific, USA and maintained in complete medium consisting of DMEM containing 10% FBS, 0.1% antibiotics-antimycotics, and kept in a humidified incubator with 5% CO_2 at 37 °C. The biocompatibility of prepared fibrous mats with and without Ag NPs was determined by incubating L-929 fibroblasts with the fibrous mats. Briefly, 10 mm^2 size of fibrous mats were transferred in 24 well plates, followed by washing with 1 mL of ethanol, and then washed twice with complete DMEM. Incubated passage 8 of L-929 cells in T75 flasks were washed twice with PBS and trypsinized using 1 mL of trypsin, followed by washing with PBS and resuspend in complete medium at 5×10^4 cell/mL. The incubated medium of washed fibrous mats was replaced with 0.5 mL of 10% DMEM followed by adding 0.5 mL of prepared cell suspension of 5×10^4 cells ml^{-1} and incubated for 1,3, and 5 days. The cell viability and metabolic behaviour of cells on fibrous mats with and without Ag NPs were

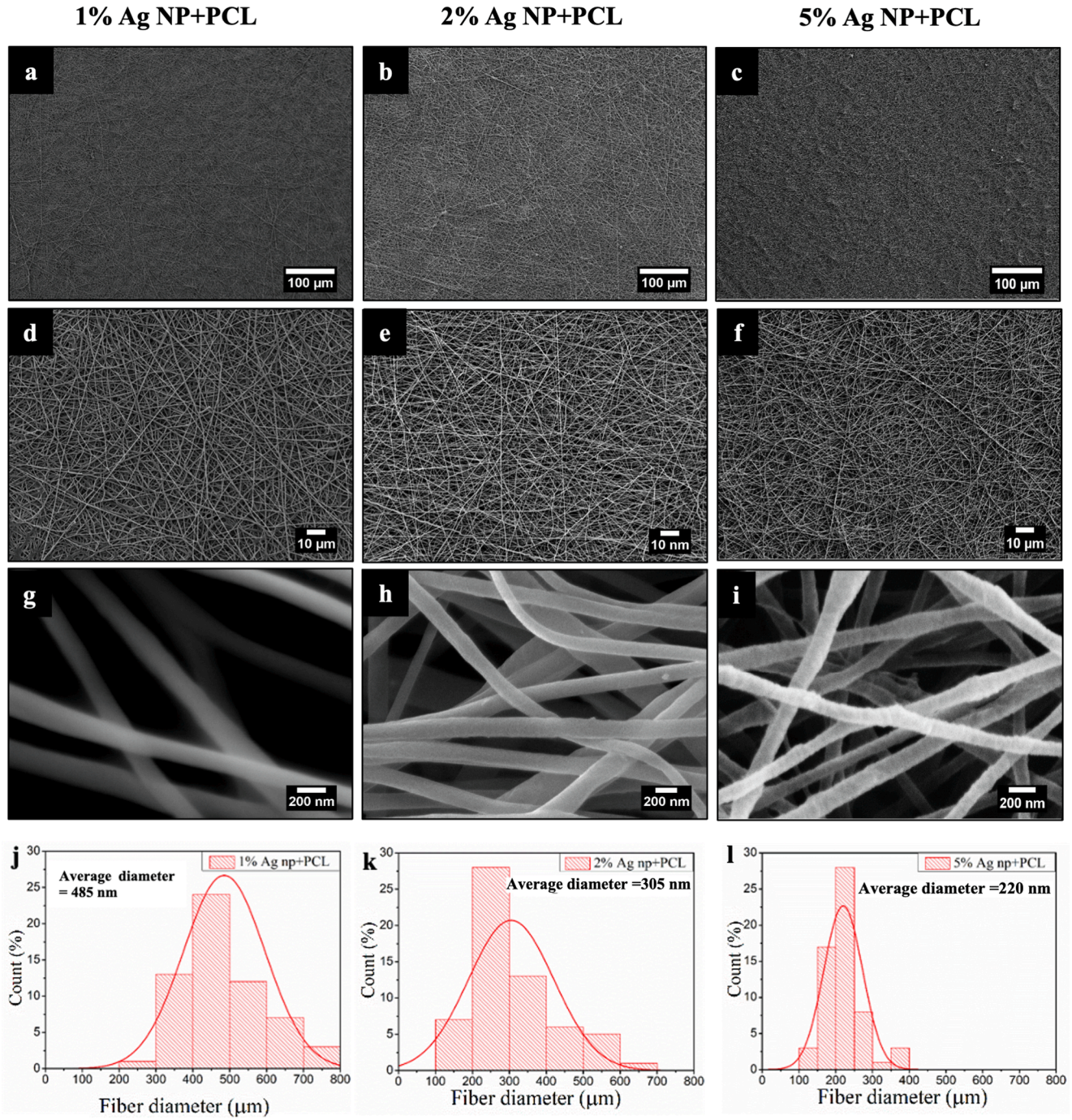

Fig. 2. SEM images of middle layer of bandage with different concentrations of Ag NPs in the PCL solution fabricated using electrospinning. Electrospun PCL fibers containing 1% (a, d, g & j), 2% (b, e, h & k) and 5% (c, f, i & l) Ag NPs wwere fabricated. Average fiber size and fiber size distribution (j, k & l) were calculated for each group. Scale bars are 100 µm (a, b and c), 10 µm (d, e and f) and 200 nm (g, h and i).

measured using the MTS assay as per manufacturer's instructions and as reported in our previously published papers [34,36]. Briefly, the media was removed from each well containing cells by using an aspirator. Cells were then immediately washed twice with PBS. After washing, 200 µL of working solution of MTS reagent was added into wells and incubated for 2.5 ± 0.05. 100 µL of mixed solution was transferred to a 96 well plate. Cell viability of prepared samples were quantified using a FLUOstar Omega microplate reader at 450 nm absorbance. The proliferation rate was calculated in % using the formula given below and considered relative to the value of the control (100%).

$$\textit{Proliferation rate}(\%) = \frac{\textit{Absorbancevalueofsample}}{\textit{Absorbancevalueofcontrol}} * 100$$

2.8. Statistical analyses

Statistical analysis of the data was performed using a two-way ANOVA using GraphPad Prism 8 software. Each experiment was performed in triplicate and are represented as mean ± SD. Values * p <0.05, **p <0.01, ***p <0.001, ****p <0.0001 were considered to be significant, ns representing non-significance. Image analysis was carried out using ImageJ software (NIH).

Table 1
Thickness of different bandages.

S. No.	Samples	Thickness of bandage (mm)	Standard Deviation (±)
1	PCL	1.8	0.2
2	1% Ag NP+PCL	1.7	0.1
3	2% Ag NP+PCL	1.7	0.1
4	5% Ag NP+PCL	1.5	0.1

3. Result and discussion

3.1. Characterization of multilayer fibrous system with Ag NP

Fig. 1 shows the SEM images of different layers of the fabricated bandage using electrospinning. The outer layer of the bandage was fabricated using 10% PS solution as shown in Fig. 1a-c. Similarly, the middle layer and inner layers were fabricated using 12% PCL (Fig. 1d-f) and 5% PEO (Fig. 1g-i), respectively. The surface of the fibers are smooth with no bead formation. The average fiber diameter was calculated using Image J software by considering 50 fibers. The average fiber diameter was found to be 5.5 ± 2 μm, 4.2 ± 3 μm and 6 ± 2 μm for PS, PCL, and PEO fibers, respectively. Fig. 1j-k shows the SEM images of PEO with the placebo drug. The fiber diameter decreased from 6 ± 2 μm to 930 ± 500 nm after adding the drug.

Fig. 2 shows the SEM images of the middle layer of the bandage i.e. PCL with different concentrations of Ag NPs with weight% of 1%, 2%, and5 % that were added to the PCL solutions, respectively. Compared to unmodified PCL fibers, the fiber diameter was reduced for fibers with Ag NPs incorporated. The average fiber diameter of control PCL fibers was 4.2 ± 3 μm, which reduced to 485 ± 350 nm, 305 ± 250 nm, and 228 ± 180 nm for fibers containing 1%, 2%, and 5% Ag NPs, respectively (Fig. 2j-l). The addition of Ag NPs to PCL electrospinning solutions increases the electrical conductivity as shown in Table S1, which resulted in an increase of surface charge of the polymer jet and hence, leads to the reduced fiber diameter [30,37]. In addition, the presence of Ag NPs on the surfaces of PCL fibers are evident from the high-resolution SEM images (Fig. 2g-i). On increasing the Ag NP concentration, not only does the fiber diameter change similarly but the surfaces of the fibers changed from smooth to rough. In Fig. 1e, PCL fibers without Ag NPs possessed a smooth surface, whereas in Fig. 2j, rough surfaces with tiny bumps were observed in PCL fibers with 5% Ag NPs. The thickness of each fibrous bandage was determined using a vernier calliper and the results were between 1.5 and 1.8 mm (Table 1). The obtained thickness for the bandage containing PCL alone was 1.8 ± 0.2, for the bandage containing 1% Ag NP+PCL was 1.8 ± 0.1, the bandage containing 2% Ag NP+PCL was 1.7 ± 0.1 and for the bandage containing 5% Ag NP+PCL was 1.5 ± 0.1. Moreover, the Ag NP incorporated bandage exhibits a rough surface texture due to the presence of Ag NPs as observed in FESEM images. Surface roughness can help improve the interactions of the scaffold with the host environment. One of the reasons is the formation of defects on the surface with increases in roughness, which provides interactions with the opposite charges from the environment and promotes chemical bonding [38].

Fig. 3 represents the characterization of the Ag NP size distribution using DLS (Fig. 3a), the Ag NP concentrations present in PCL solution using UV spectrometry (Fig. 3b), presence of different Ag NPs in PCL using XRD (Fig. 3c), along with FTIR (Fig. 3d), and release profiles of Ag ions or nanoparticles from the fiber using ICP-OES (Fig. 3e). To find the average particle size of the Ag NPs, DLS was performed using the Ag NP suspension as shown in Fig. 3a. The average hydrodynamic diameter and PDI were obtained from number average and they were found to be 64 ± 0.168 nm. In addition, the UV absorbance curve shows the absorbance spectra of different bandage solutions with and without Ag NPs. The absorbance band around 400 to 500 nm corresponds to Ag NPs. With increases in Ag NP content, the absorbance band intensity increases as observed in the case of 1% Ag NP+PCL, 2% Ag NP+PCL, and 5% Ag NP+PCL. The absence of an absorbance band around 400 to 500 nm in the case of PCL is due to the lack of Ag NPs. The presence of Ag NPs in the PCL solutions is also confirmed by the colour of the solutions; without Ag NPs it was colourless and with the increasing concentration of Ag NPs the colour of solution became light brown to dark brown [31].

Fig. 3c shows XRD patterns of the middle layer of electrospun bandages i.e., PCL with different concentrations of Ag NPs with a weight % of 1%, 2%, 5% and PCL alone. All the samples show a reflection at 21.3° and 23.6° which corresponds to the (1 1 0) and (2 0 0) crystal planes of PCL [39]. Also, PCL samples with different concentrations of Ag NPs shows low intensity peaks near 38.2° and 44.0° which corresponds to (1 1 1) and (2 0 0) crystal peaks of Ag NPs [40]. However, Ag NP peaks are not so prominent due to the small weight % of Ag NPs in the PCL solution, and this is clearer from the zoomed-out image of the XRD pattern. This confirms the presence of Ag in the PCL fibers.

The FTIR spectral analysis of 1% Ag NP+PCL, 2%Ag NP+PCL, and 5% Ag NP+PCL was performed (Fig. 3d) and the spectra displayed different vibrational stretches between 400 and 4000 cm^{-1}. All samples showed characteristic peaks of PCL including the CH_2 group rocking at 720 cm^{-1}, whereas peaks between 800 and 1100 cm^{-1} represent the C—O—C symmetric stretching. Peaks of PCL between 1100 and 1540 cm^{-1} are for C—C, C—O, O—C—O stretching, and C—H scissoring, and symmetric deformation were observed, whereas peaks between 1650 and 1750 cm^{-1} represented the C═O stretching. Other characteristic peaks of PCL between 2750 and 2850 cm^{-1} are for C-H_2 symmetric stretching, and peaks at 2850–2950 cm^{-1} for C-H_2 asymmetric stretching were also observed. The characteristic peak of Ag NPs between 3300 and 3400 cm^{-1} for O—H asymmetrical stretching vibrations was observed in 5 % Ag NP + PCL, which could be due to absorption of moisture on the highly reactive surface of the Ag NPs. Peaks expected for Ag NPs at around 1200 cm^{-1}, 1600 cm^{-1}, and 2900 cm^{-1}, were overlapping with PCL peaks [40,41].

In Fig. 3e, the in vitro release behaviour of Ag^+ ions from the PCL fibers containing Ag NPs at different concentrations was performed in PBS at pH 7.4 and 37 °C under continuous gentle shaking, followed by determining the total Ag concentration periodically using ICP-OES. In the time period up to 84 days, PCL fibers with 5% Ag NPs had the most sustained and highest Ag^+ ions release concentration (4800 ± 650 ppm/mL) compared with 1% and 2% Ag NP, which were shown to be relatively similar with a sustained cumulative release of Ag^+ ions (1000 ± 540 ppm/mL and 1800 ± 420 ppm/mL, respectively) during the incubation period of >80 days in PBS. 5% Ag NP loaded PCL fibers had a large Ag^+ ion release, which was released continuously as the fibers degraded, which is an excellent property for long-lasting antimicrobial activity. But this large release of Ag^+ ions from PCL fibers with 5% Ag NP can be cytotoxic and harmful to the wounded environment of skin tissue regeneration and may delay the wound healing. Burst kind of release profile for Ag^+ ions was observed between 70 and 77 days in 2 % and 5% Ag NP+PCL fibers, whereas after 77 days, Ag^+ ions showed a sustained release profile in 1%, 2% and 5% Ag NP+PCL fibers. As expected for this Ag NP-PCL type of system, the initial release of Ag from 1% Ag NP+PCL, 2% Ag NP+PCL and 5% Ag NP+PCL could be due to the diffusion of Ag NPs and/or Ag^+ ions from the Ag NPs deposited at or near the surface of PCL fibers during the electrospinning process, which subsequently facilitated release into the media. Whereas, the second release phase, which was showing a gradual increase in the release of Ag^+ ions, can be possible due to the generation pores on the surface of nanofibers and increased surface area facilitating the exposure to the release media followed by the leaching of Ag^+ ions. These results that demonstrated slow PCL degradation due to its hydrophobicity and the Ag NPs and/or Ag ions release mechanism from the hydrophobic nanofibers [41].

The degradation of the different fibers systems and cumulative release profile of Ag ions were analysed for the period of 84 days (Fig. S1

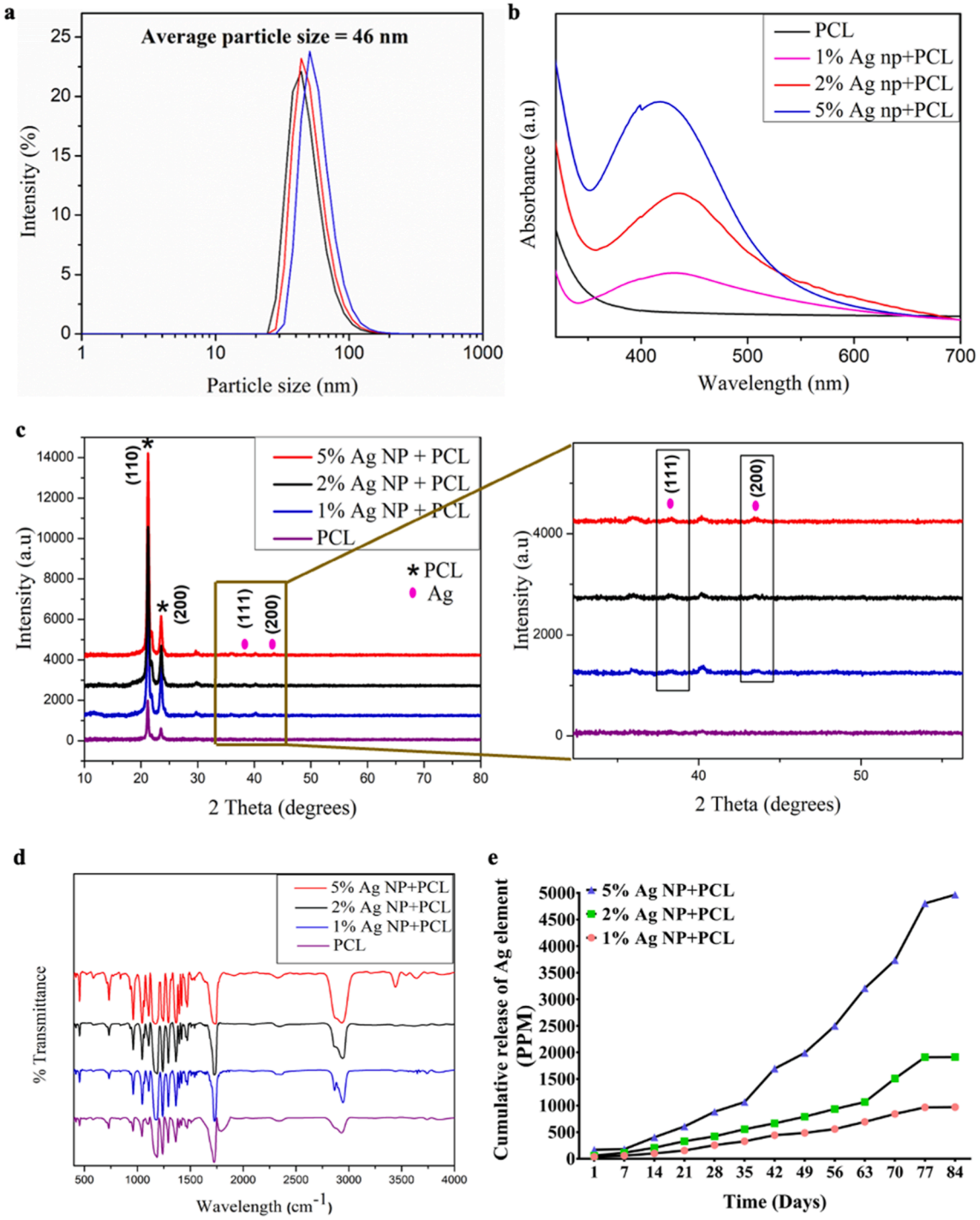

Fig. 3. Characterization of Ag NP and electrospun bandages containing different concentrations of Ag NPs with PCL. **(a)** Average particle size distribution for Ag NPs was measured using DLS. **(b)** UV absorbance of different bandage solutions with and without Ag NPs. **(c)** XRD patterns of PCL, 1% Ag NP+PCL, 2% Ag NP + PCL, and 5% Ag NP+PCL. (d) FTIR analysis of the different bandages. **(e)** Release profile of Ag ions from different fibrous bandages containing 1%, 2%, and 5% Ag NPs in PCL fibers was performed in physiological mimicking media (PBS) at various time points and determined using ICP-OES.

and Fig. 3e, respectively). During the study, the 5% Ag NP+PCL fibers degraded relatively faster than the 0% and 1% Ag NP+PCL fibers (Fig. S1). There was 97.34 ± 0.7% and 93.65 ± 0.7% weight loss observed in the PCL fiber samples with 5% and 2% Ag NP, respectively, whereas 84 ± 0.5 % and 70.56 ± 1 % total weight loss were found in samples with 1% and 0% Ag NP, respectively. The rate of degradation of the developed multilayer fibrous system is expected to be suitable as a scaffold system for regeneration of different tissue such as skin where the rate of their degradation is higher or similar with the rate of *de novo* tissue formation [42].

Fig. 4(a and b) shows the WCA measurements of the outer and inner sides of the bandage. The outer layer which consist of polystyrene is hydrophobic with a WCA of 145°. The WCA changed to 141° after 30 s of water droplet on the surface of polystyrene. The photograph in Fig. 4a also indicates the hydrophobic nature of the polystyrene. In addition, the inner layer i.e., PEO showed a WCA of 132°. However, the WCA

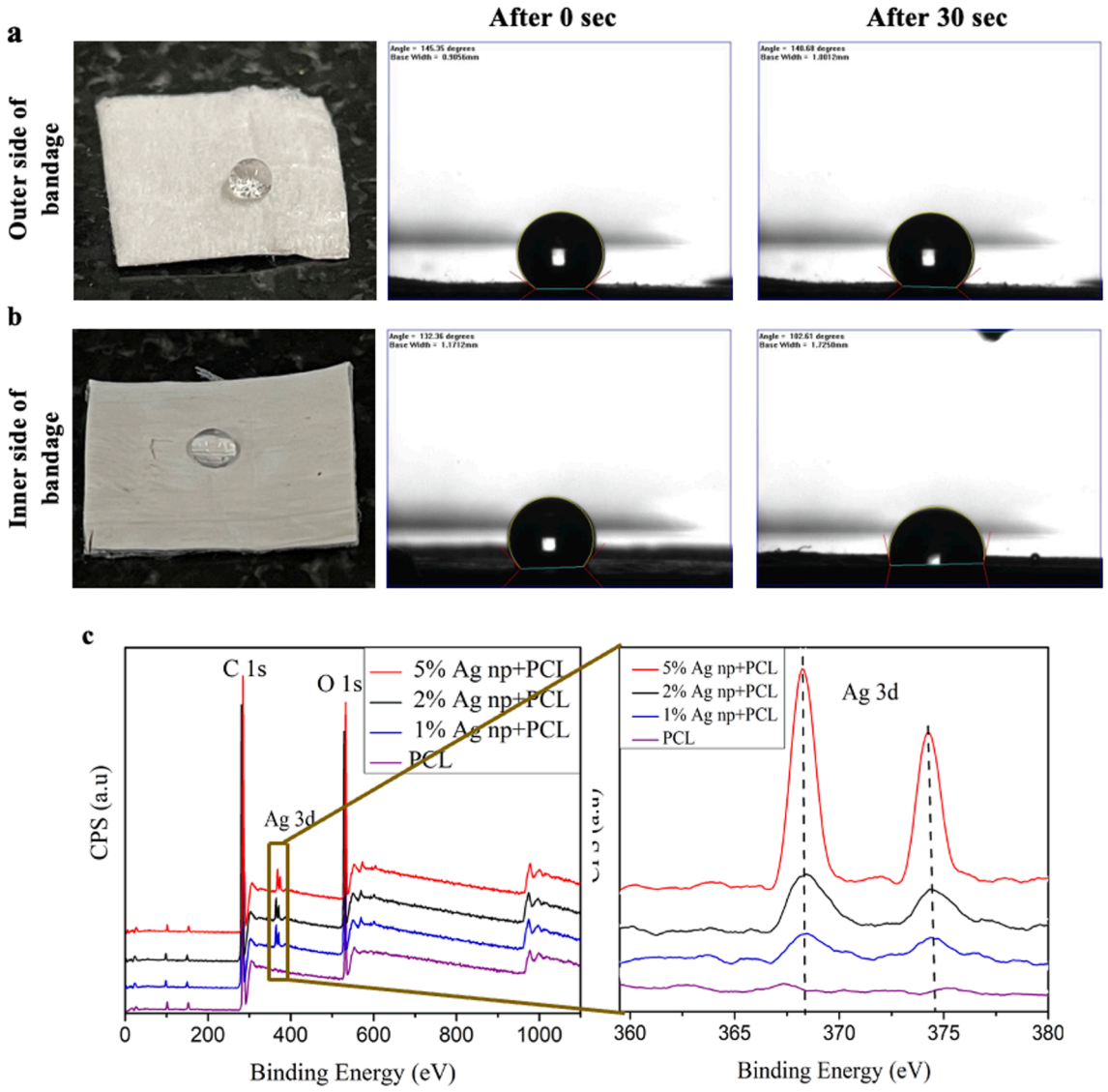

Fig. 4. Characterization of electrospun bandages containing different concentrations of Ag NPs within PCL. **(a** and **b)** Water contact angle measurement of outer layer fabricated with PS (a) and the inner layer consisted of PEO (b). **(c)** XPS wide scan and Ag 3d core-level spectra of each bandage with different concentrations of Ag NPs.

Table 2
XPS elemental composition of bandage with different concentration of Ag NP.

S. No.	Samples	C %	O %	Ag %	Si %
1	PCL	80.3 ± 1	16.8 ± 0.7	0	2.7 ± 0.4
2	1% Ag NP+PCL	77.9 ± 0.1	20.8 ± 0.1	0.08 ± 0.01	1.08 ± 0.07
3	2% Ag NP+PCL	78.6 ± 0.8	20.3 ± 0.7	0.22 ± 0.03	0.77 ± 0.1
4	5% Ag NP+PCL	78.1 ± 0.1	19.8 ± 0.1	0.45 ± 0.04	1.6 ± 0.08

decreased to 103° after 30 s on the surface of the PEO. PEO is a hydrophilic polymer, and the reason for high WCA is may be due to the high roughness of the electrospun fiber and also, the inner layer is in contact with the middle layer i.e., PCL which is hydrophobic in nature. The exposed PEO layer with PCL may also give rise to a higher WCA. The presence of a hydrophobic polystyrene outer layer acts as a protective layer by helping in waterproofing and restricting the attachment of dust and external liquids. Also, it helps in inhibiting microbial adhesion. The inner hydrophilic layer made of PEO helps in burst release of drugs, which provides fast healing of wounds. Also, facilitating cell attachment, migration, proliferation and tissue growth [43].

The elemental analysis of the electrospun fibers was determined using XPS. The XPS results (Table 2) confirm the presence of C, O and Ag in all the Ag NP loaded fibers. The increase in Ag content matched the increase in both Ag 3d peak intensity (Fig. 4c) and atomic percentage.

Table 3
Porous characteristics of PCL, 1% Ag NP+PCL, 2% Ag NP+PCL, and 5% Ag NP+PCL.

S. No.	Samples	Pore volume (cm^3g^{-1})	Pore diameter (A°)	Surface area (m^2g^{-1})
1	PCL	1.086 ± 0.024	32.16 ± 0.4	138.776 ± 2
2	1% Ag NP+PCL	0.892 ± 0.028	31.55 ± 0.2	143.989 ± 1.7
3	2% Ag NP+PCL	0.876 ± 0.018	30.99 ± 0.1	154.367 ± 2.2
4	5% Ag NP+PCL	0.851 ± 0.06	30.27 ± 0.1	165.879 ± 3

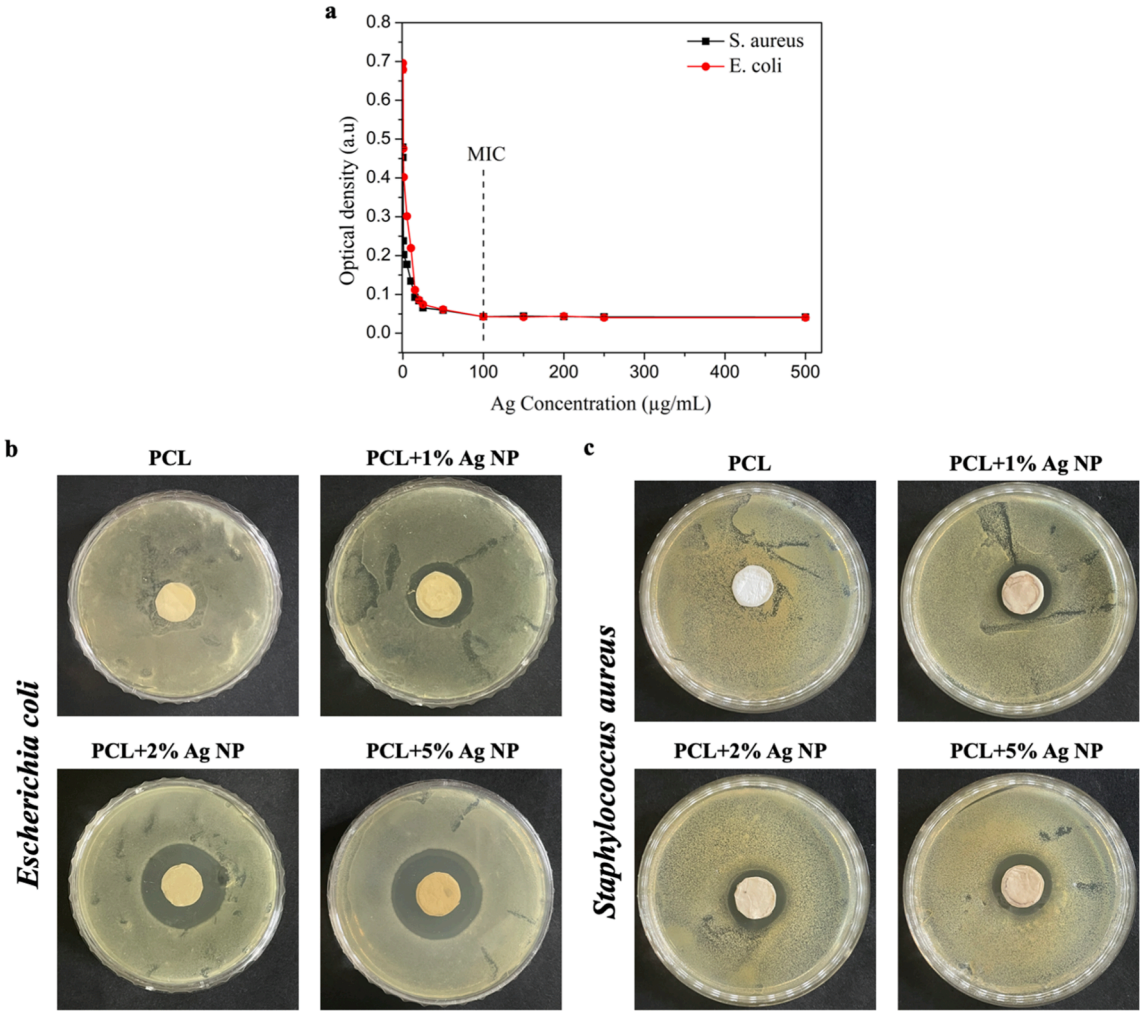

Fig. 5. Determination of the antibacterial activity of Ag NP solutions and electrospun bandages with and without Ag NPs of different concentration. **(a)** Graph showing the MIC of Ag NPs against *E. coli* and *S. aureus*. **(b** and **c)** the zone of inhibition for *E. coli* and *S. aureus* determined for different bandages with and without Ag NPs of different concentration.

The low level of Ag detected does not reflect the actual content of Ag in the fibers due to the XPS probe depth (10 nm) and there is the likelihood that the PCL covers up the Ag NPs attenuating the Ag signal. Despite this, there is a clear difference between samples with variable Ag NPs loadings.

The pore volume and pore size distribution for PCL, 1% Ag NP+PCL, 2% Ag NP+PCL, and 5% Ag NP+PCL was determined using the BJH method as shown in Table 3. It was observed that with the increase in Ag NP concentration, pore volume decreased due to blocking the pores of PCL. The change in pore volume further confirms the presence of Ag NPs on the surface of PCL. Moreover, with increased Ag NP concentration the surface area of fibers also increased. PCL alone, which consists of 12% (w/v) PCL solution in chloroform:DMF, had a pore volume ~1.086 cm^3/g with an average pore size of ~32.00 Å, and surface area of 138.776 m^2/g, whereas 1% Ag NP+PCL, which was made up of 12% (w/v) PCL with 1% (w/w) Ag NP solution represented ~0.892 cm^3/g of pore volume with an average pore size of 31.55 Å, and 143.989 m^2/gm of surface area. On the other hand, 2% Ag NP+PCL prepared using 12% (w/v) PCL with 2% (w/w) Ag NP solution in chloroform:DMF showed ~0.876 cm^3/g pore volume with an average pore size of 30.99 Å, and 154.367 m^2/gm of surface area. As expected, fibers prepared using 12% (w/v) PCL with 5% Ag NP solution exhibited ~0.851 cm^3/g of pore volume with an average pore size of 30.27 Å and 165.879 m^2/g of surface area (Table 3).

Table 4
Zone of inhibition.*

Microorganism	PCL	1% Ag NP+PCL	2% Ag NP+PCL	5% Ag NP+PCL
E. coli	0	1.32 ± 0.2	1.95 ± 0.1	2.05 ± 0.2
S. aureus	0	1.37 ± 0.05	1.40 ± 0.2	1.42 ± 0.4

* all measurements are in cm.

3.2. Antibacterial activity

A fibrous system can mimic ECM nanofibrous morphology by supporting cell attachment, proliferation, migration and tissue repair, but the major concerns that limit the success of a biomaterial are microbial colonisation and potential lack of cytocompatibility. To incorporate antimicrobial properties, Ag NPs are suitable candidates, which can be released from the fibers in the form of Ag NPs and/or Ag^+ ions, adhere to the bacteria and form 'pits' by accumulating inside the membrane [30,31]. Ag NPs are known to have broad spectrum antimicrobial activity and possess strong anti-bacterial activity [31]. For antibacterial activity studies, the most frequent etiological agents used are Gram-negative (*E. coli*) and Gram-positive*(S. aureus)* bacteria [44]. *E.coli* and *S. aureus* are most common and frequent causes of health associated infectious diseases. *E. coli* and *S. aureus* can invade the human immunity

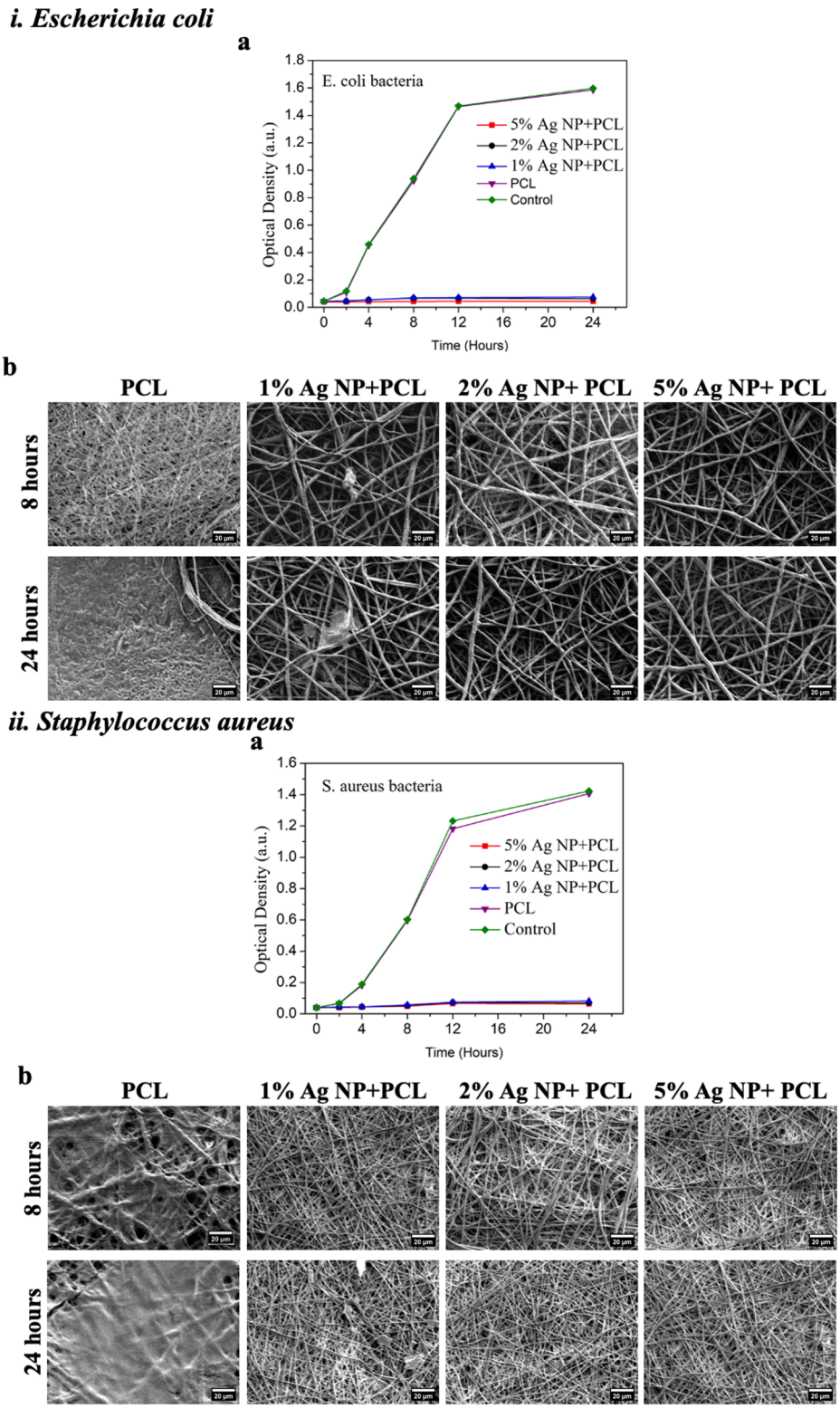

Fig. 6. Determination of the time dependent antibacterial effect of electrospun bandages with and without Ag NPs at different concentrations. *E. coli* (i) and *S aureus* (ii) were incubated with different bandages for different time points. (**a** and **c)** Graph representing the time dependent bacterial cell growth inhibition by different bandages with and without Ag NPs. (**b** and **d)** SEM images of different bandages containing 0, 1, 2 and 5% Ag NP after 8 and 24h of incubation with different bacterial cells. Scale bar for all SEM images is 20 μm.

system easily and can take the opportunity to cause infection. They are also very prone to developing multi-resistance against antibiotics.

In Fig. 5 and Table 4, the MIC and antibacterial activity (Fig. 5a) of the electrospun bandages with and without Ag NPs are shown by determining the zone of inhibition (Fig. 5b and c), quantified using the disc diffusion method. To determine the lowest effective antimicrobial concentration of Ag NPs, an MIC assay (Fig. 5a) was performed with *E. coli* and *S. aureus* for different Ag NP concentrations (0 to 500 μg/mL). The bacterial strains used for the antimicrobial study are recommended for in vitro susceptibility testing [44]. The MIC of Ag NPs with a concentration range from 1 μg/mL to 500 μg/mL was performed and observed to have a > 50% reduction in absorbance with respect to the control (0.483 for *E. coli* and 0.698 for *S. aureus*) at 5 μg/mL (0.179 for *E. coli* and 0.305 for *S. aureus*). The MIC value of Ag NPs for *E. coli* and for *S. aureus* was observed at 100 μg/mL. The concentration of Ag NPs for a microorganism growth reduction of >50% also depends on the type of

Table 5
Determination of the % growth inhibition of *E. coli* with time.

S.No.	Samples	% inhibition for *E. coli*					
		0 h	2 h	4 h	8 h	12 h	24 h
1	**PCL**	5.12 ± 0.003	10.34 ± 0.002	1.42 ± 0.003	1.76 ± 0.003	0.27 ± 0.001	0.70 ± 0.002
2	**1% Ag NP+PCL**	48.71 ± 0.001	81.61 ±	95.26 ± 0.001	96.02 ± 0.002	98.04 ± 0.002	98.97 ± 0.002
3	**2% Ag NP+PCL**	58.97 ± 0.002	83.91 ± 0.005	95.26 ± 0.001	96.24 ± 0.003	98.32 ± 0.001	99.42 ± 0.001
4	**5% Ag NP+PCL**	71.79 ± 0.002	87.36 ± 0.003	96.44 ± 0.004	96.24 ± 0.002	98.53 ± 0.003	99.67 ± 0.002

Table 6
Determination of the % inhibition of *S. aureus* with time.

S.No.	Samples	% inhibition for *S. aureus*					
		0 h	2 h	4 h	8 h	12 h	24 h
1	**PCL**	33.33 ± 0.005	48.48 ± 0.003	4.46 ± 0.004	0.88 ± 0.003	4.19 ± 0.005	1.15 ± 0.003
2	**1% Ag NP+PCL**	70.37 ± 0.005	80.30 ± 0.001	91.72 ± 0.002	96.63 ± 0.002	98.65 ± 0.004	98.12 ± 0.001
3	**2% Ag NP+PCL**	77.77 ± 0.001	83.33 ± 0.002	92.36 ± 0.001	97.34 ± 0.001	98.82 ± 0.001	98.26 ± 0.002
4	**5% Ag NP+PCL**	88.88 ± 0.002	86.36 ± 0.0020	92.35 ± 0.003	98.04 ± 0.002	98.57 ± 0.001	98.70 ± 0.001

microorganism. In Fig. 5b and Fig. 5c, *E. coli* and *S. aureus* were incubated for 24 h with 0%, 1%, 2%, and 5% of Ag NP containing PCL bandages and analysed for antibacterial efficiency. The clear zones were observed for all the Ag NP loaded bandages. The ZOI increased with an increase in the Ag content in the fibers. For *E. coli*, the highest ZOI of 2.05 ± 0.2 cm was observed with bandages containing 5% Ag NP+PCL, and 1.95 ± 0.1 cm was measured with a bandage containing 2% Ag NP+PCL (Table 4). The ZOI observed for bandages with 1% Ag NP+PCL and PCL alone are 1.32 ± 0.2 cm and 0 cm, respectively (Table 4). Similarly, for *S. aureus*, the highest ZOI of 1.42 ± 0.5 cm was observed with the bandage containing 5% Ag NP and 1.40 ± 0.2 cm was measured with a bandage containing 2% Ag NP, whereas bandages with 1% Ag NP and PCL alone had a ZOI of 1.37 ± 0.05 cm and 0 cm, respectively (Table 4). The clear zone of inhibition observed in 1% Ag NP loaded bandage confirms that even the lowest Ag NP concentration (1% Ag NP+PCL) showed effective antibacterial activity (Fig. 5b and c).

Furthermore, in Fig. 6, the time dependent inhibition study was performed up to 24 h to determine the antibacterial efficiency of different bandages. The bacterial growth kinetics on the different samples with and without Ag NPs were studied by considering the two important factors: exposure time and Ag NP concentration. The optical density for each sample was determined by measuring the absorbance at every time point (0, 2, 4, 8, 12 and 24 h). The % growth inhibition of *E. coli* was measured to be 48.71 ± 0.001% for 1% Ag NP+PCL, 58.97 ± 0.002% for 2% Ag NP+PCL, and 71.79 ± 0.002% for 5% Ag NP+PCL samples at 0 h (exposure time is 10 mins), whereas at the same time point, only 5.12 ± 0.003% inhibition was observed for the blank PCL in comparison with the control. (Table 5). Similarly (Table 6), the % growth inhibition of *S. aureus* was measured with and without 1% Ag NP+PCL (70.37 ± 0.005% inhibition), 2% Ag NP+PCL (77.77 ± 0.001% inhibition), 5% Ag NP+PCL (88.88 ± 0.002% inhibition) and PCL alone (33.33 ± 0.005% inhibition) at 0 h (exposure time is 10 mins). Within 2 h, >80% growth inhibition was observed in all samples with Ag NPs, and after 24 h >98% growth inhibition for both the microorganism (*E. coli* and *S. aureus*) was measured in comparison to the control group (Fig. 6, Table 5 and Table 6).

According to the reported mechanisms of action, Ag^+ ions and/or nanoparticles can adhere to bacterial cells and form pits. Then these accumulated Ag^+ ions and/or nanoparticles can enhance the membrane permeability and damage DNA by penetrating the bacterial cells by binding to thiol groups (–SH) present in enzymes, leading to cellular enzyme structural changes, which further prevent cell division and DNA replication. Also, during the these excessive harmful stimuli, the metabolic activity of bacteria are affected increasing the production of reactive oxygen species, which leads to an imbalance between oxidation and antioxidant systems causing bacterial cell damage [45]. The major advantages of Ag NPs compared to other antimicrobial agents are they are easy to incorporate into polymers without losing any antimicrobial properties and the release profile can be modulated [30,31]. At the same time, the antibacterial activity is directly related to the size and the available concentration of the nanoparticles [46,47]. Smaller nanoparticles exhibit enhanced antibacterial activity, and sizes <20 nm can have low MIC values, whereas larger nanoparticles (>80 nm) can have high MICs and prevent infection from several microorganisms [45]. Our developed bandage systems contained Ag NP of 20–70 nm in size and showed constant release of Ag^+ ions or Ag NPs (Fig. 4e), which effectively inhibit bacterial growth.

3.3. Cell attachment, proliferation and metabolic activity

In Fig. 7, cell attachment, biocompatibility and proliferation and metabolic activity on different electrospun fibers is shown. L-929 fibroblasts were seeded on bandage samples containing 0, 1, 2 and 5% Ag NP for time periods up to 5 days and the proliferation rate and cell viability were determined using the MTS assay. As shown in Fig. 7a, the 2% and 5% Ag NP group were unable to promote cell attachment and proliferation during the culture period, indicating that beyond 1% of Ag NP loading with respect to total weight of 3-layer bandage, the fibers are intrinsically cytotoxic and not able to achieve desirable cell attachment, migration and proliferation. At day 1 of cell culture on the different bandages, 95 ± 2% of cell growth on 0% and 1% Ag NP, 74 ± 3% on 2% Ag NP, and <40% on 5% Ag NP, respectively were observed compared to control TCPS. Furthermore, at day 3 and 5, cell growth on 0% and 1% Ag NP bandages was >90 % compared to TCPS, whereas <40% cell growth occurred on 2% and 5% Ag NP containing fibers. Day 5 cell morphologies on different fibers were determined using SEM (Fig. 7b), and live and dead staining of cells was performed at day 1, 3 and 5, was observed using confocal microscopy (Fig. 7c), followed by quantification of the live (green signals) and dead (red signals) cell proportion using ImageJ software (Table 7).

L-929 fibroblasts cultured on 0%, 1% and 2% Ag NP bandages showed good adhesion and cells had an elongated morphology, and this increased with culture time. However, no significant difference was observed in terms of cell adhesion and growth on 2% and 5% Ag NP fibers. Cell growth extensively depends on the micro-environment provided externally and considering the high amount of Ag^+ ions released from 2% and 5% Ag NP containing fibers into the growth media this can be a reason for the observed cell behaviour and cytotoxicity.

Multilayer fibrous systems can avoid the direct contact of Ag NPs with wounds and can balance biocompatibility and antimicrobial

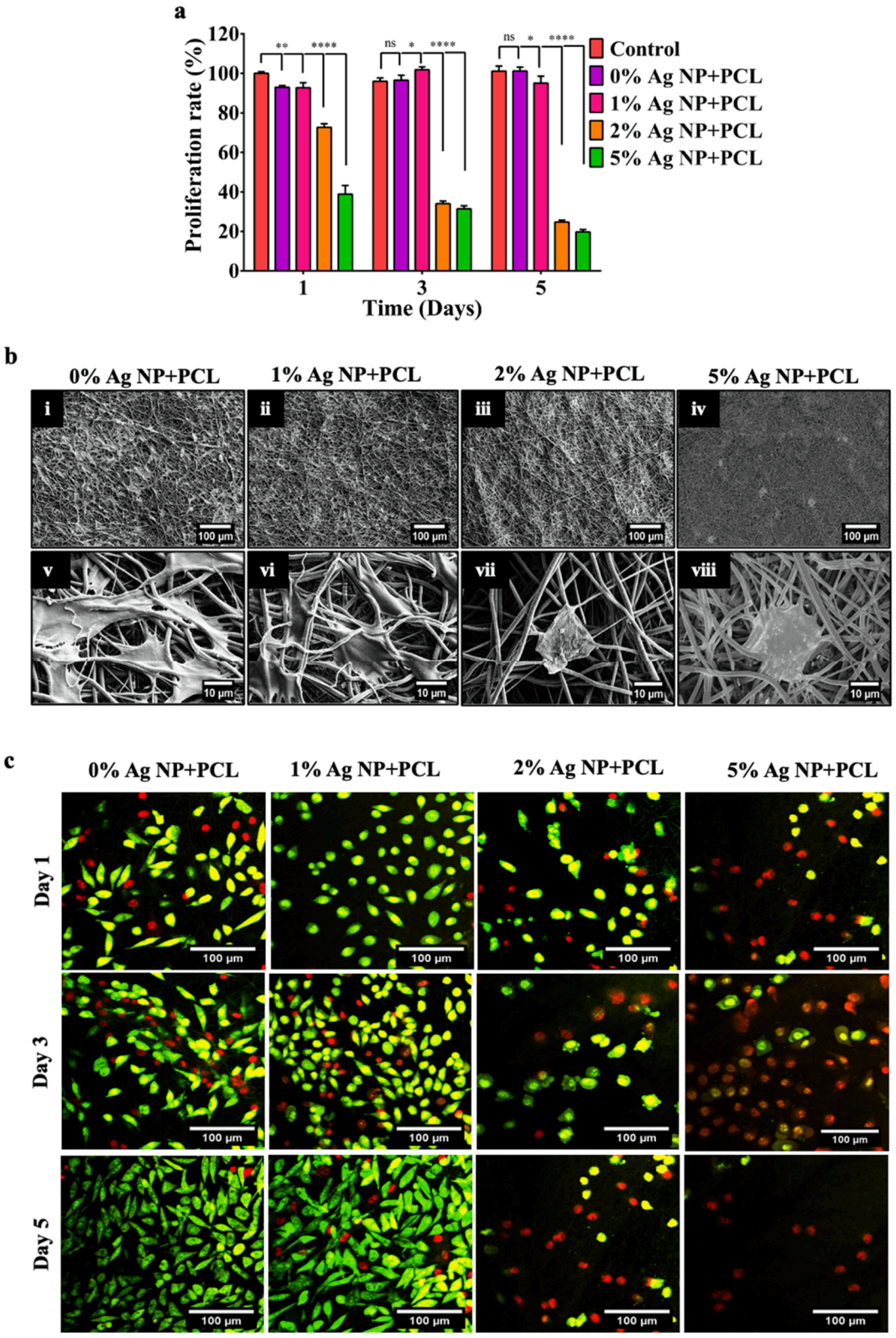

Fig. 7. Determination of in vitro cellular attachment and metabolic activity of L-929 fibroblast cells with different electrospun fibers. **(a)** L-929 cells were incubated with bandages containing 0, 1, 2 and 5% Ag NPs for 5 days and cellular proliferation activity at day 1, 3 and 5 was measured using the MTS assay. **(b)** SEM images of different bandages containing 0, 1, 2 and 5% Ag NPs after 5 days incubation with attached cells. **(c)** Attached cells on different bandages containing 0, 1, 2 and 5% Ag NP at day 1, 3 and 5 was stained using live/dead staining kit and images were captured using confocal microscope. Scale bars are 10 µm (b) and 100 µm (c).

Table 7
Quantification of live and dead L929 cells on 5th day of incubation on different samples.

S. No.	Samples	Total no of cell/ image	Live cells (%)	Dead cells (%)
1	PCL	359 ± 20	98.9 ± 0.5	1.1 ± 0.5
2	1% Ag NP+PCL	368 ± 17	98.3 ± 1	1.7 ± 0.5
3	2% Ag NP+PCL	119 ± 21	32.4 ± 2	67.6 ± 4
4	5% Ag NP+PCL	58 ± 18	17.24 ± 4	82.76 ± 5

activity [48]. Taking the release profile of Ag NPs into consideration, higher concentrations of Ag^+ ions are toxic to cells. Steady and sustained release with a multilayer fibrous (1% Ag NP+PCL) system can be less cytotoxic as compared to sustained but a large concentration of released Ag^+ ions from the 2% and 5% Ag NP+PCL fiber systems. According to the literature, Ag NPs are cytotoxic above 10 μg/ml on direct application [15] but with the fibrous system, up to 1000 ppm can be non-toxic to cells [49].

Currently, Ag NPs are typically incorporated into fibrous bandages via encapsulating Ag NPs into electrospun solutions for electrospinning to obtain Ag NP incorporated in nanofiber mats [33]. The triple layer fibrous bandage with Ag NPs in the middle layer can reduce cytotoxicity because of the sieving effect of the fibrous arrangement created due by the multilayer system [48].

4. Conclusion

We prepared and optimized a three-layered fibrous bandage with antimicrobial and biocompatible properties for use in wound healing. The outermost layer of PS was hydrophobic, which can enhance mechanical strength of bandage system and additionally protect the bandage from external moisture, minimizing the incursion and the adhesion of microorganisms. The middle layer of PCL was specifically fabricated with variable concentrations of Ag NPs, all of which effectively killed major pathogens of interest, namely *E. coli* and *S. aureus*. The inner hydrophilic layer of PEO was designed to be the point of contact with the wound site and facilitate cell attachment and migration, which leads to increased cell proliferation aimed at enhancing wound healing. Additionally, the 2% and 5% Ag NP containing bandages demonstrated higher Ag release and excellent in vitro antimicrobial activity but were more cytotoxic than bandages containing 1% Ag NPs, which had superior biocompatibility. Overall, our results demonstrate that the design of Ag NP containing antibacterial materials requires judicious choice of fabrication conditions in order to minimise potential toxic side effects.

CRediT authorship contribution statement

Nandini Sarviya: Writing – review & editing, Writing – original draft, Data curation, Investigation, Formal analysis, Methodology. **Urbashi Mahanta:** Writing – review & editing, Writing – original draft, Data curation, Investigation, Formal analysis, Methodology. **Alexander Dart:** Data curation, Investigation, Formal analysis, Methodology. **Jyotsnendu Giri:** Supervision, Writing – review & editing, Validation. **Atul Suresh Deshpande:** Supervision, Writing – review & editing, Validation. **Mudrika Khandelwal:** Supervision, Writing – review & editing, Validation. **Mrinal Bhave:** Supervision, Writing – review & editing, Validation, Funding acquisition. **Peter Kingshott:** Conceptualization, Supervision, Writing – review & editing, Validation, Formal analysis, Methodology, Funding acquisition.

Declaration of Competing Interest

The authors declare that they have no known competing financial interests or personal relationships that could have appeared to influence the work reported in this paper.

Data availability

Data will be made available on request.

Acknowledgments

This work was supported by Swinburne University of Technology funded Australian Government Research Training Program Scholarship. Swinburne University of Technology and Indian Institute of Technology Hyderabad are acknowledged as institutions in which work was carried out in.

References

[1] K. Moore, R. McCallion, R.J. Searle, M.C. Stacey, K.G. Harding, Prediction and monitoring the therapeutic response of chronic dermal wounds, Int. Wound J. 3 (2) (2006) 89–98, https://doi.org/10.1111/j.1742-4801.2006.00212.x.
[2] H. Wounds, I. Burden, An updated compendium of estimates, Adv. Wound Care 8 (2) (2019) 39–48, https://doi.org/10.1089/wound.2019.0946.
[3] G. Han, R. Ceilley, Chronic wound healing: a review of current management and treatments, Adv. Ther. 34 (3) (2017) 599–610, https://doi.org/10.1007/s12325-017-0478-y.
[4] M.B. Dreifke, A.A. Jayasuriya, A.C. Jayasuriya, Current wound healing procedures and potential care, Mater. Sci. Eng. C 48 (2015) 651–662, https://doi.org/10.1016/j.msec.2014.12.068.
[5] A. Memic, T. Abudula, H.S. Mohammed, K. Joshi Navare, T. Colombani, S. A. Bencherif, Latest progress in electrospun nanofibers for wound healing applications, ACS Appl. Bio Mater. 2 (3) (2019) 952–969, https://doi.org/10.1021/acsabm.8b00637.
[6] T.J. Sill, H.A. von Recum, Electrospinning: applications in drug delivery and tissue engineering, Biomaterials 29 (13) (2008) 1989–2006, https://doi.org/10.1016/j.biomaterials.2008.01.011.
[7] M.J. Mochane, T.S. Motsoeneng, E.R. Sadiku, T.C. Mokhena, J.S. Sefadi, Morphology and properties of electrospun PCL and its composites for medical applications: a mini review, Appl. Sci. 9 (11) (2019) 2205.
[8] A.P. Kishan, E.M. Cosgriff-Hernandez, Recent advancements in electrospinning design for tissue engineering applications: a review, J. Biomed. Mater. Res. A 105 (10) (2017) 2892–2905, https://doi.org/10.1002/jbm.a.36124.
[9] S.B. Mahjour, X. Fu, X. Yang, J. Fong, F. Sefat, H. Wang, Rapid creation of skin substitutes from human skin cells and biomimetic nanofibers for acute full-thickness wound repair, Burns 41 (8) (2015) 1764–1774, https://doi.org/10.1016/j.burns.2015.06.011.
[10] K. Ma, S. Liao, L. He, J. Lu, S. Ramakrishna, C.K. Chan, Effects of nanofiber/stem cell composite on wound healing in acute full-thickness skin wounds, Tissue Eng. A 17 (9-10) (2011) 1413–1424.
[11] M. Mostafa, N.G. Kandile, M.K. Mahmoud, H.M. Ibrahim, Synthesis and characterization of polystyrene with embedded silver nanoparticle nanofibers to utilize as antibacterial and wound healing biomaterial, Heliyon 8 (1) (2022) e08772.
[12] R. Singh, F. Ahmed, P. Polley, J. Giri, Fabrication and characterization of core-shell nanofibers using a next-generation airbrush for biomedical applications, ACS Appl. Mater. Interfaces 10 (49) (2018) 41924–41934, https://doi.org/10.1021/acsami.8b13809.
[13] A. Rajak, D.A. Hapidin, F. Iskandar, M.M. Munir, K. Khairurrijal, Electrospun nanofiber from various source of expanded polystyrene (EPS) waste and their characterization as potential air filter media, Waste Manag. 103 (2020) 76–86, https://doi.org/10.1016/j.wasman.2019.12.017.
[14] I. Unalan, B. Slavik, A. Buettner, W.H. Goldmann, G. Frank, A.R. Boccaccini, Physical and antibacterial properties of peppermint essential oil loaded poly (ε-caprolactone) (PCL) electrospun fiber mats for wound healing, Front. Bioeng. Biotechnol. 7 (2019), Original Research. doi: 10.3389/fbioe.2019.00346.
[15] S. Arab-Ahmadi, S. Irani, H. Bakhshi, F. Atyabi, B. Ghalandari, Immobilization of carboxymethyl chitosan/laponite on polycaprolactone nanofibers as osteoinductive bone scaffolds, Polym. Adv. Technol. 32 (2) (2021) 755–765, https://doi.org/10.1002/pat.5128.
[16] N. Tra Thanh, M. Ho Hieu, N. Tran Minh Phuong, T. Do Bui Thuan, H. Nguyen Thi Thu, V.P. Thai, T. Do Minh, H. Nguyen Dai, V.T. Vo, H. Nguyen Thi, Optimization and characterization of electrospun polycaprolactone coated with gelatin-silver nanoparticles for wound healing application, Mater. Sci. Eng. C 91 (2018) 318–329.
[17] A.J. Hassiba, M.E. El Zowalaty, T.J. Webster, A.M. Abdullah, G.K. Nasrallah, K. A. Khalil, A.S. Luyt, A.A. Elzatahry, Synthesis, characterization, and antimicrobial properties of novel double layer nanocomposite electrospun fibers for wound

dressing applications, Int. J. Nanomed. 12 (2017) 2205–2213, https://doi.org/10.2147/IJN.S123417 PubMed.
[18] M. Bin Ahmad, J.J. Lim, K. Shameli, N.A. Ibrahim, M.Y. Tay, Synthesis of silver nanoparticles in chitosan, gelatin and chitosan/gelatin bionanocomposites by a chemical reducing agent and their characterization, Molecules 16 (9) (2011) 7237–7248.
[19] M. Santoro, A.M. Tatara, A.G. Mikos, Gelatin carriers for drug and cell delivery in tissue engineering, J. Control. Release 190 (2014) 210–218, https://doi.org/10.1016/j.jconrel.2014.04.014.
[20] Z. Kharat, M. Amiri Goushki, N. Sarvian, S. Asad, M.M. Dehghan, M. Kabiri, Chitosan/PEO nanofibers containing Calendula officinalis extract: Preparation, characterization, in vitro and in vivo evaluation for wound healing applications, Int. J. Pharm. 609 (2021), 121132, https://doi.org/10.1016/j.ijpharm.2021.121132.
[21] D. Porrelli, M. Mardirossian, L. Musciacchio, M. Pacor, F. Berton, M. Crosera, G. Turco, Antibacterial electrospun polycaprolactone membranes coated with polysaccharides and silver nanoparticles for guided bone and tissue regeneration, ACS Appl. Mater. Interfaces 13 (15) (2021) 17255–17267, https://doi.org/10.1021/acsami.1c01016.
[22] J.G. Fernandes, D.M. Correia, G. Botelho, J. Padrão, F. Dourado, C. Ribeiro, S. Lanceros-Méndez, V. Sencadas, PHB-PEO electrospun fiber membranes containing chlorhexidine for drug delivery applications, Polym. Test. 34 (2014) 64–71, https://doi.org/10.1016/j.polymertesting.2013.12.007.
[23] T. Maver, M. Kurečič, D.M. Smrke, K.S. Kleinschek, U. Maver, Electrospun nanofibrous CMC/PEO as a part of an effective pain-relieving wound dressing, J. Sol-Gel Sci. Technol. 79 (3) (2016) 475–486, https://doi.org/10.1007/s10971-015-3888-9.
[24] W.K. Son, J.H. Youk, T.S. Lee, W.H. Park, The effects of solution properties and polyelectrolyte on electrospinning of ultrafine poly(ethylene oxide) fibers, Polymer 45 (9) (2004) 2959–2966, https://doi.org/10.1016/j.polymer.2004.03.006.
[25] Y.-Q. Wan, J.-H. He, J.-Y. Yu, Y. Wu, Electrospinning of high-molecule PEO solution, J. Appl. Polym. Sci. 103 (6) (2007) 3840–3843, https://doi.org/10.1002/app.25472.
[26] R. Augustine, N. Kalarikkal, S. Thomas, Electrospun PCL membranes incorporated with biosynthesized silver nanoparticles as antibacterial wound dressings, Appl. Nanosci. 6 (3) (2016) 337–344, https://doi.org/10.1007/s13204-015-0439-1.
[27] M. Mohseni, A. Shamloo, Z. Aghababaie, H. Afjoul, S. Abdi, H. Moravvej, M. Vossoughi, A comparative study of wound dressings loaded with silver sulfadiazine and silver nanoparticles: In vitro and in vivo evaluation, Int. J. Pharm. 564 (2019) 350–358, https://doi.org/10.1016/j.ijpharm.2019.04.068.
[28] J.S. Kim, E. Kuk, K.N. Yu, J.-H. Kim, S.J. Park, H.J. Lee, S.H. Kim, Y.K. Park, Y. H. Park, C.-Y. Hwang, Y.-K. Kim, Y.-S. Lee, D.H. Jeong, M.-H. Cho, Antimicrobial effects of silver nanoparticles, Nanomed. Nanotechnol. Biol. Med. 3 (1) (2007) 95–101.
[29] J.Y. Chun, H.K. Kang, L. Jeong, Y.O. Kang, J.-E. Oh, I.-S. Yeo, S.Y. Jung, W.H. Park, B.-M. Min, Epidermal cellular response to poly(vinyl alcohol) nanofibers containing silver nanoparticles, Colloids Surf. B Biointerfaces 78 (2) (2010) 334–342, https://doi.org/10.1016/j.colsurfb.2010.03.026.
[30] W.K. Son, J.H. Youk, T.S. Lee, W.H. Park, Preparation of Antimicrobial Ultrafine Cellulose Acetate Fibers with Silver Nanoparticles, Macromol. Rapid Commun. 25 (18) (2004) 1632–1637, https://doi.org/10.1002/marc.200400323.
[31] R. Thomas, K.R. Soumya, J. Mathew, E.K. Radhakrishnan, Electrospun polycaprolactone membrane incorporated with biosynthesized silver nanoparticles as effective wound dressing material, Appl. Biochem. Biotechnol. 176 (8) (2015) 2213–2224, https://doi.org/10.1007/s12010-015-1709-9.
[32] Y. Zhao, Y. Zhou, X. Wu, L. Wang, L. Xu, S. Wei, A facile method for electrospinning of Ag nanoparticles/poly (vinyl alcohol)/carboxymethyl-chitosan nanofibers, Appl. Surf. Sci. 258 (22) (2012) 8867–8873, https://doi.org/10.1016/j.apsusc.2012.05.106.
[33] L. Du, H.Z. Xu, T. Li, Y. Zhang, F.Y. Zou, Fabrication of ascorbyl palmitate loaded poly(caprolactone)/silver nanoparticle embedded poly(vinyl alcohol) hybrid nanofibre mats as active wound dressings via dual-spinneret electrospinning, RSC Adv. 7 (50) (2017) 31310–31318, https://doi.org/10.1039/C7RA03193A.
[34] N. Sarviya, S.M. Basu, R. Mani, M. Chauhan, P. Kingshott, J. Giri, Biomimicking nanofibrous gelatin microspheres recreating the stem cell niche for their ex-vivo expansion and in-vivo like differentiation for injectable stem cell transplantation, Biomater. Adv. 139 (2022), 212981, https://doi.org/10.1016/j.bioadv.2022.212981.
[35] H. Adeli, M.T. Khorasani, M. Parvazinia, Wound dressing based on electrospun PVA/chitosan/starch nanofibrous mats: Fabrication, antibacterial and cytocompatibility evaluation and in vitro healing assay, Int. J. Biol. Macromol. 122 (2019) 238–254, https://doi.org/10.1016/j.ijbiomac.2018.10.115.
[36] N. Sarviya, S.M. Basu, V. Induvahi, J. Giri, Laponite-gelatin nanofibrous microsphere promoting human dental follicle stem cells attachment and osteogenic differentiation for non-invasive stem cell transplantation, Macromol. Biosci. n/a (n/a), 2200347, doi: 10.1002/mabi.202200347.
[37] S. Huang, L. Zhou, M.-C. Li, Q. Wu, Y. Kojima, D. Zhou, Preparation and properties of electrospun poly (vinyl pyrrolidone)/cellulose nanocrystal/silver nanoparticle composite fibers, Materials 9 (7) (2016) 523.
[38] M.K. Ahmed, A.A. Menazea, A.M. Abdelghany, Blend biopolymeric nanofibrous scaffolds of cellulose acetate/ε-polycaprolactone containing metallic nanoparticles prepared by laser ablation for wound disinfection applications, Int. J. Biol. Macromol. 155 (2020) 636–644, https://doi.org/10.1016/j.ijbiomac.2020.03.257 From NLM.
[39] Y. Qian, Z. Zhang, L. Zheng, R. Song, Y. Zhao, Fabrication and characterization of electrospun polycaprolactone blended with chitosan-gelatin complex nanofibrous mats, J. Nanomater. 2014 (2014) 1, doi: 10.1155/2014/964621.
[40] P. Dubey, B. Bhushan, A. Sachdev, I. Matai, S. Uday Kumar, P. Gopinath, Silver-nanoparticle-Incorporated composite nanofibers for potential wound-dressing applications, J. Appl. Polym. Sci. 132 (35) (2015) n/a–n/a.
[41] J. Johnson, A. Niehaus, S. Nichols, D. Lee, J. Koepsel, D. Anderson, J. Lannutti, Electrospun PCL in vitro: a microstructural basis for mechanical property changes, J. Biomater. Sci. Polym. Ed. 20 (4) (2009) 467–481, https://doi.org/10.1163/156856209X416485.
[42] C.A. Simmons, E. Alsberg, S. Hsiong, W.J. Kim, D.J. Mooney, Dual growth factor delivery and controlled scaffold degradation enhance in vivo bone formation by transplanted bone marrow stromal cells, Bone 35 (2) (2004) 562–569, https://doi.org/10.1016/j.bone.2004.02.027.
[43] B. Yu, C. He, W. Wang, Y. Ren, J. Yang, S. Guo, Y. Zheng, X. Shi, Asymmetric wettable composite wound dressing prepared by electrospinning with bioinspired micropatterning enhances diabetic wound healing, ACS Appl. Bio Mater. 3 (8) (2020) 5383–5394, https://doi.org/10.1021/acsabm.0c00695.
[44] M. Cobos, I. De-La-Pinta, G. Quindós, M.J. Fernández, M.D. Fernández, Graphene oxide-silver nanoparticle nanohybrids: synthesis, characterization, and antimicrobial properties, Nanomaterials 10 (2) (2020) 376.
[45] Y. Dong, H. Zhu, Y. Shen, W. Zhang, L.i. Zhang, A. Mukherjee, Antibacterial activity of silver nanoparticles of different particle size against Vibrio Natriegens, PLoS One 14 (9) (2019) e0222322.
[46] J.R. Morones, J.L. Elechiguerra, A. Camacho, K. Holt, J.B. Kouri, J.T. Ramírez, M. J. Yacaman, The bactericidal effect of silver nanoparticles, Nanotechnology 16 (10) (2005) 2346–2353, https://doi.org/10.1088/0957-4484/16/10/059.
[47] R. Das, S. Gang, S.S. Nath, Preparation and antibacterial activity of silver nanoparticles, J. Biomater. Nanobiotechnol. 2 (4) (2011) 472–475.
[48] C. He, X. Liu, Z. Zhou, N. Liu, X. Ning, Y. Miao, Y. Long, T. Wu, X. Leng, Harnessing biocompatible nanofibers and silver nanoparticles for wound healing: sandwich wound dressing versus commercial silver sulfadiazine dressing, Mater. Sci. Eng. C 128 (2021), 112342, https://doi.org/10.1016/j.msec.2021.112342.
[49] M. Pérez-Díaz, E. Alvarado-Gomez, M. Magaña-Aquino, R. Sánchez-Sánchez, C. Velasquillo, C. Gonzalez, A. Ganem-Rondero, G. Martínez-Castañon, N. Zavala-Alonso, F. Martinez-Gutierrez, Anti-biofilm activity of chitosan gels formulated with silver nanoparticles and their cytotoxic effect on human fibroblasts, Mater. Sci. Eng. C 60 (2016) 317–323, https://doi.org/10.1016/j.msec.2015.11.036.